Superconductivity, magnetism, and stoichiometry of single crystals of $Fe_{1+y}(Te_{1-x}S_x)_z$

Rongwei Hu,[1,*] Emil S. Bozin,[1,2] J. B. Warren,[3] and C. Petrovic[1]
[1]*Condensed Matter Physics and Materials Science Department, Brookhaven National Laboratory, Upton, New York 11973, USA*
[2]*Department of Applied Physics and Applied Mathematics, Columbia University, New York, New York 10027, USA*
[3]*Instrumentation Division, Brookhaven National Laboratory, Upton, New York 11973, USA*
(Received 21 August 2009; revised manuscript received 15 November 2009; published 11 December 2009)

We report synthesis of high-quality $Fe_{1+y}(Te_{1-x}S_x)_z$ single crystals and a comprehensive study of structural, magnetic, and transport properties. We demonstrate the very small upper critical field anisotropy of $Fe_{1+y}(Te_{1-x}S_x)_z$, $\gamma_H = H_{c2}^{\|c}/H_{c2}^{\perp c}$. The value of γ_H reaches 1.05 at $T=0.65T_C$ for $Fe_{1.12}Te_{0.83}S_{0.11}$ while still maintaining large values of upper critical field. There is high sensitivity to material stoichiometry which includes vacancies on the Te(S) site. Our results reveal competition and coexistence of magnetic order and percolative superconductivity for $x \geq 0.03$ while zero resistivity is achieved for $x \geq 0.1$.

DOI: 10.1103/PhysRevB.80.214514 PACS number(s): 74.62.Bf, 74.10.+v, 74.20.Mn, 74.70.Dd

I. INTRODUCTION

The discovery of superconductivity in quaternary iron-based layered superconductor $LaFeAsO_{1-x}F_x$ with $T_C = 26$ K stimulated an intense search for superconductors with higher T_C in this materials class.[1] Shortly after, the critical temperatures were raised up to 55 K in materials of the ZrCuSiAs structure type,[2] and superconductivity had been discovered in $Ba_{1-x}K_xFe_2As$ and LiFeAs.[3,4] Superconductivity in the PbO-type FeSe opened another materials space in the search for iron-based superconductors.[5] This was followed by the discovery of superconductivity in polycrystalline $FeTe_{1-x}Se_x$ and $FeTe_{1-x}S_x$.[6,7] Binary iron chalcogenide superconductors share the most prominent characteristics of iron arsenide compounds: a square-planar lattice of Fe with tetrahedral coordination similar to LaFeAsO or LiFeAs, and Fermi-surface topology.[8] They crystallize in a simple crystal structure which is amenable to modeling by band-structure calculations.[5,7–12]

Iron pnictide superconductors exhibit Cooper pairing in proximity to a magnetic ground state, similar to all exotic superconductors: cuprate oxides, heavy fermion intermetallics and organics. The magnetism in these materials is strongly influenced by subtle crystal structure changes.[1,13,14] FeSe hosts high T_c's of up to 37 K under pressure and an isotropic superconducting (SC) state. Its crystal structure changes from high-temperature tetragonal $P4/nmm$ to low-temperature orthorhombic $Cmmm$ at 70 K.[15,16] In $Fe_{1.08}Te$ transition to monoclinic space group $P21/m$ with commensurate antiferromagnetic (AF) order occurs between 65 and 75 K, whereas $Fe_{1.14}Te$ exhibits weaker first-order transition to orthorhombic space group $Pmmm$ and incommensurate AF order from 55 to 63 K.[9]

It was noted, however, that it would be desirable to have isotropic superconductors with high T_c and ability to carry high critical currents for power applications.[17] In this work we report the synthesis of $Fe_{1+y}(Te_{1-x}S_x)_z$ superconducting single crystals for $x=(0-0.15)$, $y=(0-0.14)$, and $z=(0.94-1)$. We demonstrate small values of $\gamma_H = H_{c2}^{\|c}/H_{c2}^{\perp c}$ while still maintaining large values of the upper critical field and critical currents. We examine the evolution of superconductivity and magnetism with S doping and provide experimental evidence for structural parameters at the magnetic/superconducting boundary.

II. EXPERIMENTAL METHOD

Single crystals of $Fe_{1+y}(Te_{1-x}S_x)_z$ were grown from Te-S self-flux using a high-temperature flux method.[18,19] Elemental Fe, Te, and S were sealed in quartz tubes under partial argon atmosphere. The sealed ampoule was heated to a soaking temperature of 430–450 °C for 24 h, followed by a rapid heating to the growth temperature at 850–900 °C, and then slowly cooled to 800–840 °C. The excess flux was removed from crystals by decanting. Platelike crystals up to $11 \times 10 \times 2$ mm^3 can be grown. Elemental analysis and microstructure was performed using energy-dispersive x-ray spectroscopy in an JEOL JSM-6500 scanning electron microscope. The average stoichiometry was determined by examination of multiple points on the crystals. Total scattering data from finely pulverized crystals were obtained at 80 K at 11-ID-B beamline of the Advanced Photon Source synchrotron using 58.26 keV x-rays ($\lambda = 0.2128$ Å) selected by a Si 311 monochromator. Two-dimensional (2D) patterns for samples in 1mm diameter Kapton tubes were collected using a MAR345 2D detector, placed perpendicular to the primary beam path, 188.592 mm away from the sample. An Oxford Cryosystem cryostream was used for temperature regulation. Details on experimental procedures, data processing, the atomic pair-distribution function (PDF) method, and structural modeling can be found elsewhere.[20–22] Flux-free rectangular shaped crystals with the largest surface orthogonal to $\hat{c}$ axis of tetragonal structure were selected for four-probe resistivity measurements with current flowing parallel to the $\hat{a}$ axis of tetragonal structure. Thin Pt wires were attached to electrical contacts made with Epotek H20E silver epoxy. Sample dimensions were measured with an optical microscope Nikon SMZ-800 with 10 μm resolution. Magnetization and resistivity measurements were carried out in a Quantum Design MPMS-5 (magnetic property measurement system) and a PPMS-9 (physical property measurement system) for temperatures from 1.8 to 350 K.

III. RESULTS

Typical synchrotron data (symbols), with fully converged $P4/nmm$ structural model superimposed (solid lines), and

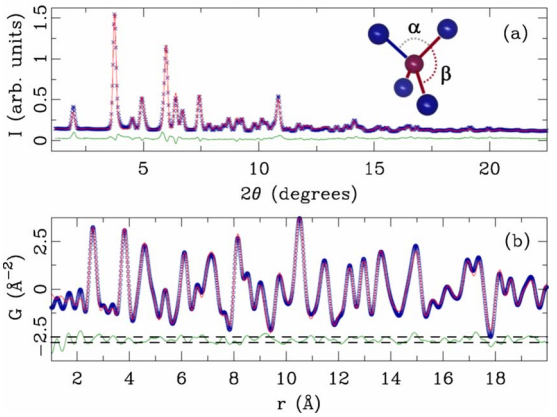

FIG. 1. (Color online) (a) $Fe_{1+y}(Te_{1-x}S_x)_z$ synchrotron Rietveld and (b) PDF refinement results taken at $T=80$ K. Inset shows two Te-Fe-Te bond angles illustrated on the $FeTe_4$ tetrahedron.

corresponding difference curves (offset for clarity) are presented in Fig. 1, featuring $Fe_{1.12}Te_{0.83}S_{0.11}$. Panel (a) features a Rietveld refinement with a corresponding PDF refinement shown in (b). The PDF is peaked at positions corresponding to the observed interatomic distances. Excellent fits with low agreement factors are obtained for all studied $Fe_{1+y}(Te_{1-x}S_x)_z$ samples. Initial PDF fits assumed ideal stoichiometry, and revealed slightly enhanced atomic displacement parameters, suggesting either Te(S) deficiency, or excess Fe content, or both. To explore this, in final $P4/nmm$ models where S shared site with Te, Fe/Te/S ratios were kept fixed at values obtained from scanning electron microscopy (SEM), while stoichiometry was refined. Additionally, Fe was allowed to occupy two sites, Fe(1) (0,0,0) and Fe(2)(0.5,0,z). Total Fe content in the refinements was constrained to respect the SEM ratio while the relative occupancy of the two Fe sites was allowed to vary. Results are reported in Table I. Undoped FeTe crystallizes with excess Fe variably occupying interstitial Fe(2) site and full occupancies of Fe(1) and Te sites. With contraction of the unit cell due to sulfur doping we observe both excess Fe and vacancies on Te(S) site. With reduction in the unit cell due to an increase in sulfur stoichiometry (x) excess Fe(y) decreases so that for highest x =0.15 we observe the smallest deviation from ideal stoichiometry. Both Fe(1) and Fe(2) sites are still occupied for high x values (Table I).

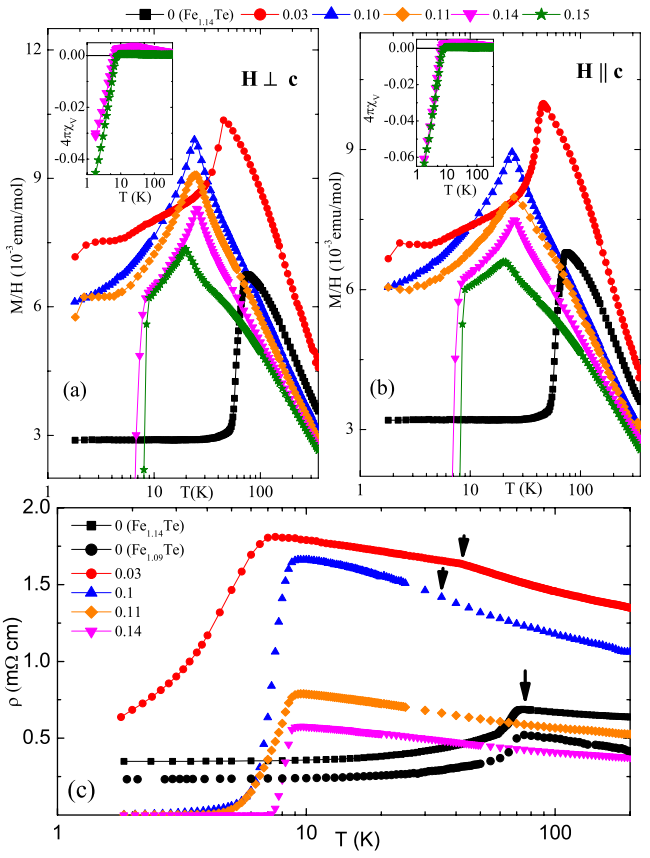

FIG. 2. (Color online) (a) Magnetic susceptibility as a function of temperature for $H\perp c$ and (b) $H\|c$. Insets show the Meissner volume fraction of $x=0.14$ and $x=0.15$. (c) In-plane resistivity in zero field for $Fe_{1+y}(Te_{1-x}S_x)_z$. Arrows show positions of peaks in $\partial\rho/\partial T$ that correspond to anomalies in magnetization associated with SDW transitions [(a) and (b)].

Figures 2(a) and 2(b) shows the anisotropic temperature dependence of magnetic susceptibility for $Fe_{1+y}(Te_{1-x}S_x)_z$ for a magnetic field of 1000 Oe applied in the ab plane and along c axis. The peak at 70 K for $Fe_{1.14(2)}Te$ corresponds to an AF transition presumably coupled with structural and first order.[23] The transition spans about 20 K for both field orientations. The magnetic susceptibility is isotropic above 70 K and $\chi^{\|c}/\chi^{\perp c}$ increases from 1 to 1.1 below the transition. The transition temperature is suppressed with sulfur doping down

TABLE I. Structural parameters from PDF refinement at $T=80$ K, magnetic and superconducting properties of $Fe_{1+y}(Te_{1-x}S_x)_z$. Transition temperatures T_1 and T_2 are from $\partial(\chi T/\partial T)$ data. Temperatures of T_C onset and zero resistance are from resistivity data.

$Fe_{1+y}(Te_{1-x}S_x)_z$	V (Å^3)	c/a	Occ(Fe1)	Occ(Fe2)	α	Θ (K)	μ (μ_B)	T_2 (K)	T_1 (K)	T_C^{onset} (K)	T_C (K)
$Fe_{1.14(2)}Te_{1.01(1)}$	91.150(4)	1.642(1)	1.04(2)	0.10(2)	117.46(1)	−191(4)	3.92(2)	59(1)	70(1)		
$Fe_{1.09(2)}Te_{1.00(1)}$	91.017(4)	1.640(1)	1.02(2)	0.07(2)			3.73(1)	59(1)	66(1)		
$Fe_{1.12(3)}Te_{0.97(1)}S_{0.03(2)}$	90.558(4)	1.637(1)	1.00(3)	0.12(3)	117.57(1)	−175(1)	3.83(1)	41(1)	44(1)	6.5(1)	
$Fe_{1.13(3)}Te_{0.85(1)}S_{0.10(2)}$	90.032(5)	1.632(1)	1.00(4)	0.13(4)	117.33(1)	−186(4)	3.56(2)	21(1)	23(1)	8.5(1)	2.0(1)
$Fe_{1.12(3)}Te_{0.83(1)}S_{0.11(2)}$	90.095(4)	1.632(1)	1.06(4)	0.07(4)	117.30(1)	−162(3)	3.38(2)		20(1)	8.6(1)	3.5(1)
$Fe_{1.06(3)}Te_{0.88(1)}S_{0.14(2)}$	90.097(4)	1.632(1)	0.95(4)	0.11(4)	117.32(1)	−156(6)	3.36(3)		23.5(1)	8.7(1)	7.0(1)
$Fe_{0.98(4)}Te_{0.90(1)}S_{0.15(2)}$	89.900(5)	1.632(1)	0.82(4)	0.16(4)	117.21(1)	−167(7)	3.34(6)		19(1)	8.8(5)	

to 20 K by $x=0.15$. A diamagnetic signal is observed for $x \geq 0.14$ [Figs. 2(a) and 2(b) insets], in apparent coexistence with a magnetic state. The volume fraction $4\pi\chi_v$ reaches $-0.06 \sim -0.09$ at 0 K by linear extrapolation. Magnetic susceptibility is Curie-Weiss type above 200 K. The effective moments estimated are between the low-spin ($2.94\mu_B$, $S=1$) and high-spin ($4.9\mu_B$, $S=2$) values of an $Fe^{2+}(3d^6)$ in a tetragonal crystal field (Table I). The high-temperature effective moments decrease with the S doping and with the reduction in excess Fe. Negative Curie-Weiss temperatures attest to the antiferromagnetic coupling between moments (Table I).

The in-plane electrical resistivity in zero field is shown in Fig. 2(c). Residual resistivity values at low temperatures for pure $Fe_{1+y}Te$ and crystals with the highest sulfur concentration x are comparable to single crystals grown by Bridgeman method,[24] but smaller by a factor of 3–4 than in polycrystalline materials[7] due to the absence of grain boundaries and secondary phases. The grain boundaries are not transparent as in MgB_2 where intrinsic low values of ρ_0 in high-quality polycrystals are often lower than in crystals.[25] Therefore grain boundaries cannot be neglected when measuring resistivity on polycrystals of iron chalcogenide superconductors. The resistivity of $Fe_{1+y}Te$ above the magnetic transition is poorly metallic, in agreement with measurements on polycrystals and an optical conductivity study which did not find a semiconducting gap.[7,26] This is an important distinction from the metallic resistivity above T_c in iron-based superconductors of $ThCr_2Si_2$, ZrCuSiAs structure, or even FeSe.[5,27–30] The magnitude of the resistivity, ρ, becomes larger with small doping for $x=0.03$ but decreases with the increase in S concentration. Two distinct contributions to ρ are observed in the low-temperature phase at the temperature of the magnetization anomaly: semiconducting and metallic or semimetallic [arrows Fig. 2(c)]. For $x=0.03$ a small decrease in temperature slope in ρ is observed whereas the resistivity of $x=0.1$ sample shows an increase, indicating that a part of the Fermi surface is destroyed. This can be understood within the framework of density-functional theory (DFT) calculations that predict a metal with "nesting" cylindrical Fermi surfaces which are separated by a wave vector corresponding to spin-density wave (SDW) low-temperature ground state.[8] With further increase in x, the resistivity anomaly at the magnetic transition is smaller and broader when compared to $x=0$. Though all samples for $x \geq 0.03$ show a clear onset of superconductivity; zero resistivity is observed for $x \geq 0.10$ [Fig. 2(c)].

The temperature dependence of resistivity with a magnetic field applied perpendicular and parallel to c axis for the superconducting sample $x=0.14$ is shown in Fig. 3(a). The residual resistivity of the normal state $\rho_0=0.58$ mΩ cm of our crystals is smaller than in polycrystalline $FeTe_{1-x}S_x$.[7] It is comparable to residual resistivity observed in $NdFeAsO_{0.7}F_{0.3}$ ($\sim$0.2 mΩ cm) (Ref. 31) or $(Ba_{0.55}K_{0.45})Fe_2As_2$($\sim$0.4 m$\Omega$ cm) (Ref. 28) single crystals. Transition width of our crystals ($\Delta T_c = T_{onset} - T_{zero\ \rho} = 1.8$ K) is smaller than that in Ref. 7 ($\Delta T_c = 2$ K). The small shift of the transition temperature with magnetic field indicates a large zero-temperature upper critical field. The upper critical field H_{c2} is estimated as the field corresponding

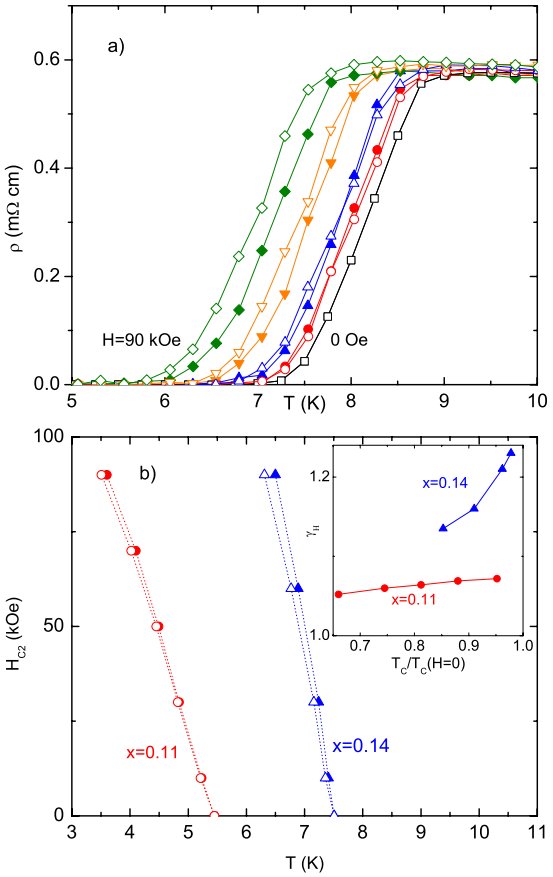

FIG. 3. (Color online) (a) In-plane resistivity for $x=0.14$ of two field orientations, $H \perp c$ (solid symbols) and $H \| c$ (open symbols). The applied magnetic field increases gradually from 0 Oe (the rightmost curve), 10 kOe, 30 kOe, 60 kO to 90 kOe (the leftmost curve). (b) The upper critical fields for $x=0.11$ and 0.14, $H \perp c$ (solid symbols) and $H \| c$ (open symbols). Dotted lines are guides to the eye. Inset shows the anisotropy in the upper critical field $\gamma_H = H_{c2}^{\|c}/H_{c2}^{\perp c}$.

to the 90% of resistivity drop. An estimate for $H_{c2}(T=0)$ is given by weak-coupling formula for conventional superconductors in the Werthamer-Helfand-Hohenberg model (Table II): $H_{c2o}(0) \sim -0.7 H'_{c2}(T_c) T_c$.[32] The superconducting coherence length $\xi(0\ \text{K})[\xi^2 = \Phi_0/2\pi H_{c2}]$ is around 3 nm. The anisotropy $\gamma_H = H_{c2}^{\|c}/H_{c2}^{\perp c}$ decreases with a temperature decrease approaching a value close to unity. By $T_c/T_c(0) \approx 0.65$ [Fig. 3(b) inset], $\gamma_H = 1.05$, for $x=0.11$. These values indicate that $Fe_{1+y}(Te_{1-x}S_x)_z$ is a high-field isotropic superconductor with γ_H smaller than that in Ref. 32 [$\gamma_H > 1.5$ at $0.5T_C(H=0)$] or in Ref. 33 [$\gamma_H \sim 1.3$ at $0.5T_C(H=0)$].

To determine the anisotropy of the critical current, we analyze the magnetic measurements using an extended Bean model.[34,35] Considering a rectangular prism-shaped crystal of dimension $c<a<b$, when a magnetic field is applied along the crystalline c axis, the in-plane critical current density j_c^{ab} is given by

$$j_c^{ab} = \frac{20}{a} \frac{\Delta M_c}{(1 - a/3b)}$$

in which ΔM_c is the width of the magnetic hysteresis loop for increasing and decreasing field. When the magnetic field

TABLE II. Upper critical field at zero temperature and corresponding coherence length for two superconducting samples.

	$H'^{\perp c}_{c2}(T_c)$	$H^{\perp c}_{c2}(0)$ (T)	$H'^{\parallel c}_{c2}(T_c)$	$H^{\parallel c}_{c2}(0)$ (T)	$\xi^{\perp c}(0)$ (nm)	$\xi^{\parallel c}(0)$ (nm)
$Fe_{1.12(3)}Te_{0.83(1)}S_{0.11(2)}$	−4.9	19	−4.6	18	4.3	4.3
$Fe_{1.06(3)}Te_{0.88(1)}S_{0.14(2)}$	−10.7	56	−8.4	44	2.4	2.7

is applied along the b axis and parallel to the ab plane, both of the in-plane j_c^{ab} and the crossplane j_c^c are involved in the Bean model. For a crystal in our measurements with $a=1.245$ mm, $b=1.285$ mm, and $c=0.732$ mm,

$$j_c^c = \frac{c}{3a}\frac{j_c^{ab}}{(1-20\Delta M_b/cj_c^{ab})}.$$

Because of the large volume fraction of the normal and magnetic state, a magnetic background is superposed on the hysteresis loop. Moreover, as shown in Fig. 4(b) inset, the hysteretic magnetization loop for the sample $x=0.14$ sustains above the superconducting transition temperature at 7.5 K and vanishes above the antiferromagnetic transition at 25 K. It implies a magnetic structure of $FeTe_{1-x}S_x$ where a ferromagnetic component coexists with an antiferromagnetic moment. Density-functional calculation on FeTe by Subedi *et al.*[8] does indicate that besides the SDW, FeTe is close to a ferromagnetic instability, similar to LaFeAsO. In order to estimate the ΔM only due to flux pinning, we take the hysteresis loop immediately above superconducting transition at 8 K as the ferromagnetic background and subtract it from other loops below 7.5 K. The identical hysteresis loops at 8 and 9 K in the normal state justifies our rationale to use them as a temperature-independent background. Figure 4(a) shows hysteresis loops for $H\|c$ and $H\perp c$ at 1.8 K after background removal. The magnetically deduced in-plane and interplane critical current density are displayed in Fig. 4(b). The ratio of j_c^{ab}/j_c^c is roughly about 4. The critical current densities for both directions are 10^5-10^6 A/cm^2, comparable to MgB_2, $Ba(Fe_{1-x}Co_x)_2As_2$ in the same temperature range.[36]

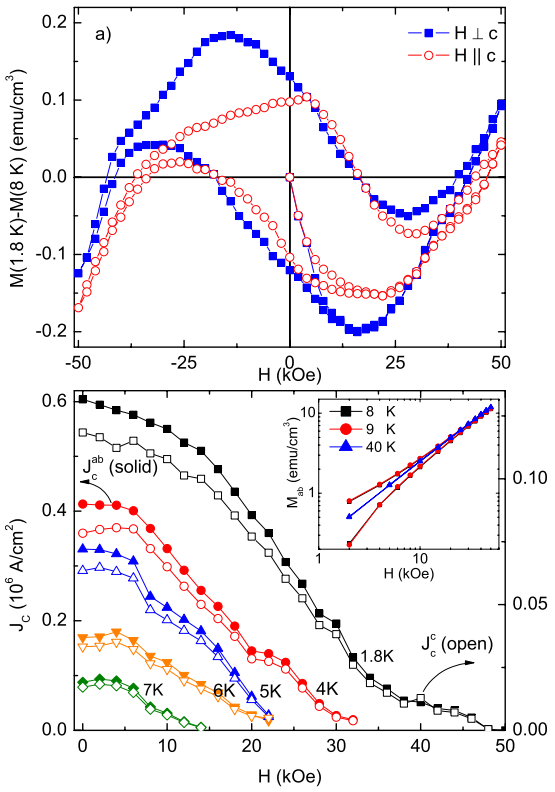

FIG. 4. (Color online) (a) Magnetization hysteresis loops of $x=0.14$ for 1.8 K after ferromagnetic background subtraction for $H\|c$ (open symbols) and $H\perp c$ (solid symbols). (b) In-plane (to left axis) and interplane (to right axis) critical currents for $x=0.14$. Inset shows the magnetization at 8, 9, and 40 K. Only the positive field magnetization is shown on log-log scale and the virgin curves of the loops at 8 and 9 K are omitted for clarity.

Figure 5(a) gives the temperature-dependent specific heat C_p and M/H for $Fe_{1.14(2)}Te$ and $Fe_{1.09(2)}Te$ below 90 K. Both crystals show two lambda anomalies at magnetic/structural transition around $T_1=70$ K and $T_2=59$ K for $Fe_{1.14(2)}Te$ and around $T_1=66$ K and $T_2=59$ K for $Fe_{1.09(2)}Te$. Above and below the transition region there is no difference in $C_p(T)$. A magnetic field of 90 kOe shifts both transition in both samples for $\Delta T=1$ K. The entropy $\Delta S=2.2$ J/mol associated with the transition is independent of the iron stoichiometry y [Fig. 5(b)]. This is smaller than estimated change in entropy in $Fe_{1.07}Te$ of $\Delta S\sim 3.2$ J/mole(K).[23] The discrepancy is probably due to conventional PPMS heat-capacity setup which introduces sizeable error in the vicinity of the first-order phase transition.[37] Nevertheless, we can still compare the change in ΔS for $Fe_{1+y}Te$ crystals with different y caused by AF contribution which dominates ΔS in the transition region.[23] Assuming that total entropy is lost on the spin-state transition $\Delta S=R\ln[(2S_H+1)/(2S_L+1)]$ and using $\mu_{eff}=\sqrt{4S(S+1)}$, high-temperature effective moment is $\mu^H_{eff}(Fe_{1.14(2)}Te)=3.92\mu_B$, $\mu^H_{eff}(Fe_{1.09(2)}Te)=3.73\mu_B$, we obtain the moment value below magnetic transitions in the ordered state $\mu^H_{eff}(Fe_{1.14(2)}Te)=1.3\mu_B$ and $\mu^H_{eff}(Fe_{1.09(2)}Te)=1.2\mu_B$. Larger relative entropy change for higher y is related to the occupancy of iron in the interstitial sites which is expected to be strongly magnetic.[11] Interestingly, these numbers are very close to values for a spin moment of $1.3\mu_B$ associated with SDW transition calculated by DFT calculations.[8]

The low-temperature C_p data for $Fe_{1.14}Te$ can be fitted to the $C(T)=\gamma T+\beta T^3$ power law below 15 K with $\gamma=32$ mJ/mole K^2 and $\beta=0.49$ mJ/mole K^4 from which a $\theta_D=228$ K can be obtained [Fig. 5(c)]. Specific heat shows a broad feature around T_c [Fig. 5(c) inset] for superconducting samples similar to other iron pnictides.[28] Due to high upper

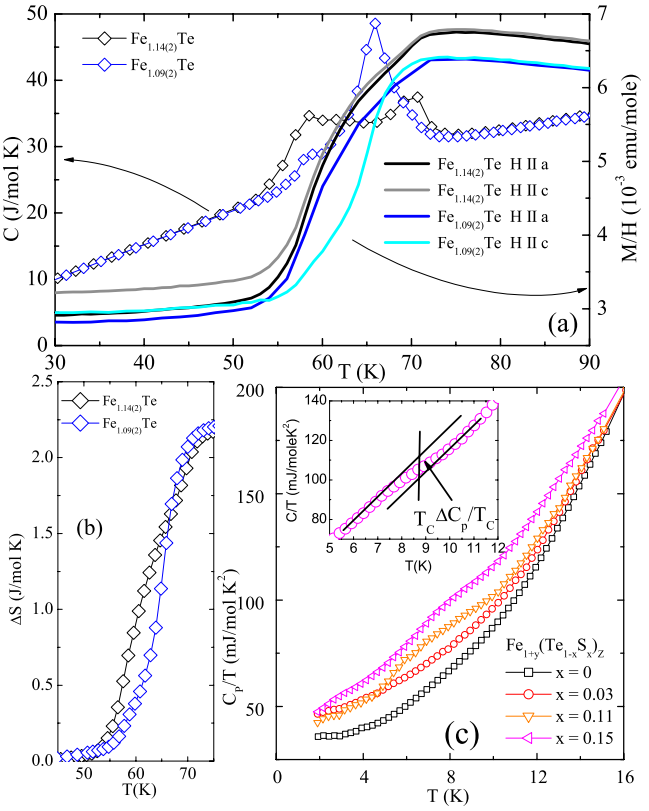

FIG. 5. (Color online) (a) Magnetization and heat capacity C_p at SDW transition of $Fe_{1.14(2)}Te$ and $Fe_{1.09(2)}Te$. (b) Entropy balance around the transition. (c) Low-temperature heat capacity with discontinuity in C_p/T at T_C for $x=0.15$ sample shown in the inset. Clear jumps associated with superconducting transitions are seen for $x \geq 0.11$.

critical fields and apparent coexistence of superconductivity and long-range magnetic order in our crystals, a reliable estimate of the normal-state contribution to electronic specific heat γ is rather difficult. Additional uncertainty in testing traditional isotropic weak-coupling BCS value of $\Delta C_p/\gamma T_c$ in $Fe_{1+y}(Te_{1-x}S_x)_z$ is introduced by the percolative nature of superconductivity with up to 7% superconducting volume fraction (Fig. 2). Therefore we restrict ourselves to an estimate of the C_p/T discontinuity associated with superconducting transition for material with the highest sulfur concentration and consequently the most pronounced jump in specific heat.[38] For $x=0.15$ it is about 12 mJ/mole K^2 at $T_c=8.8$ K, comparable to what is observed in $Ba(Fe_{1-x}Co_x)_2As_2$ and $Ba(Fe_{1-x}Ni_x)_2As_2$ single crystals.[38]

Closer inspection of the $(\partial\chi T/\partial T)$ (Ref. 39) and $\partial\rho/\partial T$ data (Fig. 6) for $Fe_{1.14(2)}Te$ and $Fe_{1.09(2)}Te$ unveils two transitions at temperatures T_1 and T_2 that correspond to specific-heat anomalies in Fig. 5(a) (Table I). With sulfur substitution both transitions are clearly observed only up to $x \leq 0.1$ (Fig. 6). For higher sulfur concentration only one broad anomaly can be observed (Fig. 6 insets). Two successive transitions were reproduced on independently grown crystals within the same batch and in different batches. The exact temperatures of transitions T_1 and T_2 did vary from batch to batch.

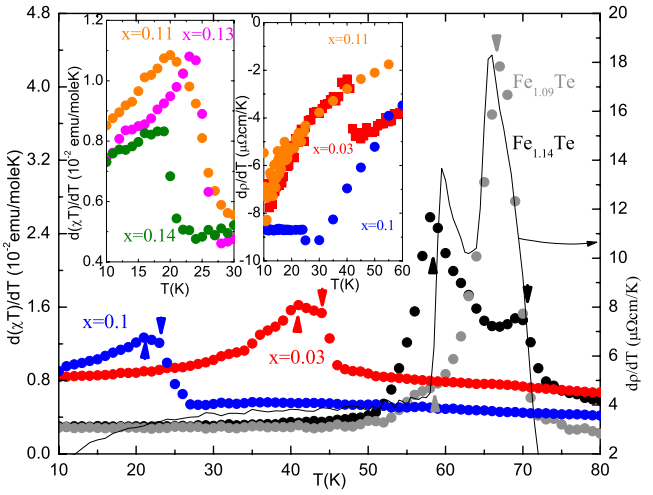

FIG. 6. (Color online) $Fe_{1.14(2)}Te$ and $Fe_{1.09(2)}Te$ as well as sulfur-doped samples for $x \leq 0.1$ show two clear magnetization anomalies around SDW transition, as seen in derivatives $d(\chi T)/dT$ and $d\rho/dT$ (inset). For higher sulfur content anomalies are broader (insets) and cannot be distinguished.

IV. DISCUSSION

The AF SDW in pure $Fe_{1+y}Te$ is accompanied by a lattice distortion for all investigated values of y as in the undoped Fe-As superconductors.[27,40–43] DFT calculations have found that excess Fe donates charge as Fe^+ to FeTe layers with strong tendency of moment formation on the excess Fe site.[11] By comparing our $C(T)$ data with the specific heat data taken on $Fe_{1.06}Te$ crystals[44] it can be seen that the clarity of the two step anomaly increases with the increase in y in $Fe_{1+y}Te$. It is absent for $Fe_{1.05}Te$ and $Fe_{1.06}Te$,[40,44] visible for $Fe_{1.09}Te$ and rather pronounced for $Fe_{1.14}Te$ with similar entropy under both transitions [Figs. 5(a) and 5(b)]. Magnetic measurements $(\partial\chi T/\partial T)$ closely match thermodynamic data (Figs. 5 and 6). Whereas temperature of lower temperature transition T_2 (59 K) does not change with change in y, $Fe_{1+y}Te$ with higher content of excess Fe y has transition T_1 at higher temperature (70 and 66 K, Table I). The Fermi level in $Fe_{1+y}Te$ lies exactly at the sharp peak of the excess Fe density of states $N(E_F)$; therefore higher T_1 may be magnetically driven based on the Stoner criterion $N(E_F)I>1$.[11] Increased ρ values for $Fe_{1.14}Te$ when compared to $Fe_{1.09}Te$ are also consistent with this (Fig. 2). Higher level of excess Fe y corresponds to larger size mismatch between cylindrical electron and hole Fermi surfaces. Therefore T_2 and T_1 transitions may correspond to successive SDW Fermi-surface nesting of individual electron-hole cylindrical pieces.[8,11] Recent work shows that the magnetic order in parent compounds of iron-based superconductors is established below temperature of structural transition with up to 20 K difference in temperature of transition, as seen in $CeFe_{1-x}Co_xAsF$.[42,45] It is unlikely that two transitions seen in our crystals correspond to individual magnetic and structural transitions since they have the same sensitivity to magnetic field.

Our findings are summarized in the electronic and structural phase diagrams shown in Fig. 7. The lattice contraction with isoelectronic sulfur substitution corresponds to a posi-

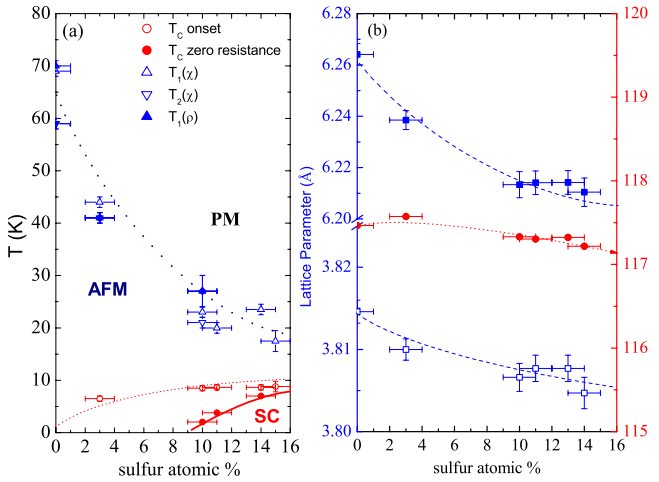

FIG. 7. (Color online) (a) Electronic phase diagram of $Fe_{1+y}(Te_{1-x}S_x)_z$, showing paramagnetic (PM), antiferromagnetic and SC ground states. Blue triangles pointing up and down correspond to T_2 and T_1 transitions, respectively. For $x=0$ both can easily be identified. Red circles denote onset of superconducting transition in ρ and zero resistance. Transition for $x=0.15$ was estimated from heat-capacity measurement. (b) Structural parameters at $T=80$ K.

tive chemical pressure. The magnetic transition is suppressed from the ~58–70 K region to about 20 K. Signatures of percolative superconductivity were observed for all $x \geq 0.3$. Zero resistivity in fully percolating path was observed for $x \geq 0.1$. The superconducting transition width decreases with the increase in x and T_c. Clearly, there is a competition between magnetic SDW order and the superconducting state since with increase in sulfur content x, $dT_{1,2}/dx$ and dT_c/dx have opposite signs.

Having delineated the evolution of magnetic and superconducting properties, it is natural to ask what is the correlation with the structural parameters. The unit-cell parameters a and c of $P4/nmm$ crystal structure decrease smoothly at $T=80$ K as sulfur is substituted in the place of tellurium (Table I). The c/a ratio decreases to nearly constant value for $x \geq 0.1$ up to $x=0.15$. After $x=0.15$ we have observed formation of FeS in the hexagonal NiAs type of structure in the same range of synthesis parameters. Close inspection of the tetrahedral angle α at $T=80$ K [Fig. 7(b)] reveals an extremum near the superconducting percolation threshold. The angle α increases up to $x=0.03$ and then decreases with further sulfur increase. The tetrahedral angle α therefore seems to be intimately connected with electronic transport properties which will be discussed next.

Both $x=0$ crystals are metallic in the low-temperature phase [Fig. 2(c)]. On the other hand, two successive transitions have also been reported in $FeTe_{0.92}$ under high pressure in the intermediate regime between $P=(1-1.8)$ GPa,[46] as well as two distinct types of transport below the magnetic and structural transition: metallic for $FeTe_{0.9}$ and semiconducting for $FeTe_{0.82}$.[10] We note that semiconducting contribution to ρ below the magnetization anomaly for $x=0.10$ and $x=0.11$ (Fig. 2) coincides with Te(S) vacancies from synchrotron x-ray refinement (Fig. 1, Table I). Crystals with no Te(S) vacancies within error bars have metallic or semimetallic contributions to ρ. This is in agreement with photoemission studies that showed no visible energy gaps at the electron and hole Fermi surface for $y<0.05$ in $Fe_{1+y}Te$.[47] Increase in resistivity at the SDW AF transition signals small gap opening at the Fermi surface. The band structure of FeTe features intersecting elliptical cylindrical electron portions at the Brillouin-zone corners compensated by hole sections with higher effective mass at the zone center.[8] Our findings show that the details of the nesting condition depend rather sensitively on the tetrahedral angle α and vacancies on the ligand site. This points to importance of hybridization between Te p and Fe d bands in addition to excess stoichiometry y on Fe site.[12] Our results strongly suggest that nanoscale inhomogeneity seems to be the key factor governing magnetic and electronic transport properties in $Fe_{1+y}(Te_{1-x}S_x)_z$.

Finally we comment on the percolative nature of superconductivity found in our crystals. Superconducting volume fraction increases with sulfur stoichiometry x. The $4\pi\chi_v$ reaches up to −0.07 at $T=1.8$ K ($\sim 0.26T_c$) for the highest x crystals where zero resistivity was observed to approach the T_c onset (Fig. 7). This is in good agreement with the polycrystalline data in Ref. 7. This signals granular superconducting state coexisting with SDW order, taking only a fraction of sample volume and stabilizing to fully percolating superconducting path by $x=0.14$. Similar coexistence was observed in other iron-based superconductors, $CaFe_{1-x}Co_xAsF$, $SmFeAsO_{1-x}F_x$, $SrFe_2As_2$, and $BaFe_2As_2$.[41,45,48] For example, in the underdoped region of $Ba_{1-x}K_xFe_2As_2$ the superconducting volume fraction has been reported to be $(23 \pm 3)\%$ of $-1/4\pi$ at $\sim 0.06T_c$ increasing up to 50% for nearly optimally doped material.[28,49,50] Since SDW magnetic order and superconductivity compete for the same Fermi surface, percolative nature of superconductivity may be associated with intrinsic mesoscopic real-space phase separation as in cuprate oxides or $CaFe_{1-x}Co_xAsF$.[45,51,52] Consequently superconductivity may be mediated by magnetic fluctuations, consistent with small values of electron-phonon coupling constant found in doped $Fe_{1+x}Te$ and FeSe.[8]

V. CONCLUSION

In conclusion, we have performed combined and comprehensive study of structural, magnetic and superconducting properties of $Fe_{1+y}(Te_{1-x}S_x)_z$ single crystals. Magnetic transition decreases from ~58–70 K to about 20 K for $x=0.15$. We have shown that the increase in excess Fe y in $Fe_{1+y}Te$ results in two anomalies in thermodynamic, magnetization, and transport properties. Electronic transport is rather sensitive to possible vacancies on Te(S) site. $Fe_{1+y}(Te_{1-x}S_x)_z$ are isotropic high-field superconductors with one of the smallest values of $\gamma_H = H_{c2}^{\parallel c}/H_{c2}^{\perp c}$ observed so far in iron-based superconducting materials. Moreover, anisotropy in the superconducting state decreases with increased sulfur content. Filamentary superconductivity is observed for all x in apparent coexistence with magnetism. Microscopic measurements such as muon-spin rotation (μSR) are needed to

confirm real-space phase separation and/or coexistence of superconductivity and magnetism. By utilizing high-pressure synthesis techniques even higher T_C's, upper critical fields and smaller γ_H may be simultaneously obtained. Since $FeTe_{1-x}S_x$ superconductors consist of relatively inexpensive and nontoxic elements, materials based on FeTeS with full volume fraction may be useful for future high-field power applications. In addition, higher S doping level would enable the answer to the question if maximal T_C occurs at the point where magnetism disappears as in cuprate oxides and other complex iron arsenide superconductors.

We are grateful for helpful discussions with Paul Canfield, Sergey Bud'ko, Simon Billinge, and Myron Strongin. This work was carried out at the Brookhaven National Laboratory, which is operated for the U.S. Department of Energy by Brookhaven Science Associates (Grant No. DE-Ac02-98CH10886). Use of the Advanced Photon Source was supported by the U. S. Department of Energy, Office of Science, Office of Basic Energy Sciences, under Contract No. DE-AC02-06CH11357. This work was supported by the Office of Basic Energy Sciences of the U.S. Department of Energy.

*Present address: Ames Laboratory US DOE and Department of Physics and Astronomy, Iowa State University, Ames, IA 50011, USA.

[1] Y. Kamihara, T. Watanabe, M. Hirano, and H. Hosono, J. Am. Chem. Soc. **130**, 3296 (2008).
[2] Z.-A. Ren, W. Lu, J. Yang, W. Yi, X.-L. Shen, Zheng-Cai, G.-C. Che, X.-L. Dong, L.-L. Sun, F. Zhou, and Z.-X. Zhao, Chin. Phys. Lett. **25**, 2215 (2008).
[3] M. Rotter, M. Tegel, and D. Johrendt, Phys. Rev. Lett. **101**, 107006 (2008).
[4] X. C. Wang, Q. Q. Liu, Y. X. LV, W. B. Gao, L. X. Yang, R. C. Yu, F. Y. Li, and C. Q. Jin, Solid State Commun. **148**, 538 (2008).
[5] F.-C. Hsu, J.-Y. Luo, K.-W. Yeh, T.-K. Chen, T.-W. Huang, P. M. Wu, Y.-C. Lee, Y.-L. Huang, Y.-Y. Chu, D.-C. Yan, and M.-K. Wu, Proc. Natl. Acad. Sci. U.S.A. **105**, 14262 (2008).
[6] K. W. Yeh, T. W. Huang, Y. L. Huang, T. K. Chen, F. C. Hsu, P. M. Wu, Y. C. Lee, Y. Y. Chu, C. L. Chen, J. Y. Luo, D. C. Yan, and M. K. Wu, EPL **84**, 37002 (2008).
[7] Y. Mizuguchi, F. Tomioka, S. Tsuda, T. Yamaguchi, and Y. Takano, Appl. Phys. Lett. **94**, 012503 (2009).
[8] A. Subedi, L. Zhang, D. J. Singh, and M. H. Du, Phys. Rev. B **78**, 134514 (2008).
[9] W. Bao, Y. Qiu, Q. Huang, M. A. Green, P. Zajdel, M. R. Fitzsimmons, M. Zhernenkov, S. Chang, M. Fang, B. Qian, E. K. Vehstedt, J. Yang, H. M. Pham, L. Spinu, and Z. Q. Mao, Phys. Rev. Lett. **102**, 247001 (2009).
[10] M. H. Fang, H. M. Pham, B. Qian, T. J. Liu, E. K. Vehstedt, Y. Liu, L. Spinu, and Z. Q. Mao, Phys. Rev. B **78**, 224503 (2008).
[11] L. Zhang, D. J. Singh, and M. H. Du, Phys. Rev. B **79**, 012506 (2009).
[12] M. J. Han and S. Y. Savrasov, Phys. Rev. Lett. **103**, 067001 (2009).
[13] I. I. Mazin and M. D. Johannes, Nat. Phys. **5**, 141 (2009).
[14] M. R. Norman, Phys. **1**, 21 (2008).
[15] S. Margadonna, Y. Takabayashi, Y. Ohishi, Y. Mizuguchi, Y. Takano, T. Kagayama, T. Nakagawa, M. Takata, and K. Prassides, Phys. Rev. B **80**, 064506 (2009).
[16] S. Margadonna, Y. Takabayashi, M. T. McDonald, K. Kasperkiewicz, Y. Mizuguchi, Y. Takano, A. N. Fitch, E. Suard, and K. Prassides, Chem. Commun. (Cambridge) **2008**, 5607.
[17] Report on of the Basic Energy Sciences, U.S. Department of Energy, Superconductivity, Washington, DC, 2006.
[18] P. C. Canfield and Z. Fisk, Philos. Mag. B **65**, 1117 (1992).
[19] Z. Fisk and J. P. Remeika, in *Handbook on the Physics and Chemistry of Rare Earths*, edited by K. A. Gschneider and J. Eyring (Elsevier, Amsterdam, 1989), Vol. 12.
[20] P. J. Chupas, X. Qiu, J. C. Hanson, P. L. Lee, C. P. Grey, and S. J. L. Billinge, J. Appl. Crystallogr. **36**, 1342 (2003).
[21] T. Egami and S. J. L. Billinge, *Underneath the Bragg Peaks: Structural Analysis of Complex Materials* (Pergamon, New York/Elsevier, Oxford, England, 2003).
[22] C. L. Farrow, P. Juhas, J. W. Liu, D. Bryndin, E. S. Bozin, J. Bloch, Th. Proffen, and S. J. L. Billinge, J. Phys.: Condens. Matter **19**, 335219 (2007).
[23] S. Li, C. de la Cruz, Q. Huang, Y. Chen, J. W. Lynn, J. Hu, Y.-L. Huang, F.-C. Hsu, K.-W. Yeh, M.-K. Wu, and P. Dai, Phys. Rev. B **79**, 054503 (2009).
[24] B. C. Sales, A. S. Sefat, M. A. McGuire, R. Y. Jin, D. Mandrus, and Y. Mozharivskyj, Phys. Rev. B **79**, 094521 (2009).
[25] R. A. Ribeiro, S. L. Bud'ko, C. Petrovic, and P. C. Canfield, Physica C **382**, 194 (2002).
[26] G. F. Chen, Z. G. Chen, J. Dong, W. Z. Hu, G. Li, X. D. Zhang, P. Zheng, J. L. Luo, and N. L. Wang, Phys. Rev. B **79**, 140509(R) (2009).
[27] M. Rotter, M. Tegel, D. Johrendt, I. Schellenberg, W. Hermes, and R. Pöttgen, Phys. Rev. B **78**, 020503(R) (2008).
[28] N. Ni, S. L. Bud'ko, A. Kreyssig, S. Nandi, G. E. Rustan, A. I. Goldman, S. Gupta, J. D. Corbett, A. Kracher, and P. C. Canfield, Phys. Rev. B **78**, 014507 (2008).
[29] A. S. Sefat, R. Jin, M. A. McGuire, B. C. Sales, D. J. Singh, and D. Mandrus, Phys. Rev. Lett. **101**, 117004 (2008).
[30] G. Wu, Y. L. Xie, H. Chen, M. Zhong, R. H. Liu, B. C. Shi, Q. J. Li, X. F. Wang, T. Wu, Y. J. Yan, J. J. Ying, and X. H. Chen, J. Phys.: Condens. Matter **21**, 142203 (2009).
[31] J. Jaroszynski, F. Hunte, L. Balicas, Y.-j. Jo, I. Raičević, A. Gurevich, D. C. Larbalestier, F. F. Balakirev, L. Fang, P. Cheng, Y. Jia, and H. H. Wen, Phys. Rev. B **78**, 174523 (2008).
[32] N. R. Werthamer, E. Helfand, and P. C. Hohemberg, Phys. Rev. **147**, 295 (1966).
[33] A. Yamamoto, J. Jaroszynski, C. Tarantini, L. Balicas, J. Jiang, A. Gurevich, D. C. Larbalestier, R. Jin, A. S. Sefat, M. A. McGuire, B. C. Sales, D. K. Christen, and D. Mandrus, Appl. Phys. Lett. **94**, 062511 (2009).
[34] C. P. Bean, Phys. Rev. Lett. **8**, 250 (1962).
[35] E. M. Gyorgy, R. B. van Dover, K. A. Jackson, L. F. Schneem-

eyer, and J. V. Waszczak, Appl. Phys. Lett. **55**, 283 (1989).
[36] M. A. Tanatar, N. Ni, C. Martin, R. T. Gordon, H. Kim, V. G. Kogan, G. D. Samolyuk, S. L. Bud'ko, P. C. Canfield, and R. Prozorov, Phys. Rev. B **79**, 094507 (2009).
[37] J. C. Lashley, M. F. Hundley, A. Migliori, J. L. Sarrao, P. G. Pagliuso, T. W. Darling, M. Jaime, J. C. Cooley, W. L. Hults, L. Morales, D. J. Thoma, J. L. Smith, J. Boerio-Goates, B. F. Woodfield, G. R. Stewart, R. A. Fisher, and N. E. Phillips, Cryogenics **43**, 369 (2003).
[38] S. L. Bud'ko, N. Ni, and P. C. Canfield, Phys. Rev. B **79**, 220516(R) (2009).
[39] M. E. Fisher, Philos. Mag. **7**, 1731 (1962).
[40] G. F. Chen, Z. Li, D. Wu, G. Li, W. Z. Hu, J. Dong, P. Zheng, J. L. Luo, and N. L. Wang, Phys. Rev. Lett. **100**, 247002 (2008).
[41] A. J. Drew, Ch. Niedermayer, P. J. Baker, F. L. Pratt, S. J. Blundell, T. Lancaster, R. H. Liu, G. Wu, X. H. Chen, I. Watanabe, V. K. Malik, A. Dubroka, M. Rossle, K. W. Kim, C. Baines, and C. Bernhard, Nature Mater. **8**, 310 (2009).
[42] C. de la Cruz, Q. Huang, J. W. Lynn, J. Li, W. Ratcliff, J. L. Zaretsky, H. A. Mook, G. F. Chen, J. L. Luo, N. L. Wang, and P. Dai, Nature (London) **453**, 899 (2008).
[43] H.-H. Klauss, H. Luetkens, R. Klingeler, C. Hess, F. J. Litterst, M. Kraken, M. M. Korshunov, I. Eremin, S.-L. Drechsler, R. Khasanov, A. Amato, J. Hamann-Borrero, N. Leps, A. Kondrat, G. Behr, J. Werner, and B. Büchner, Phys. Rev. Lett. **101**, 077005 (2008).
[44] S. L. Bud'ko, P. C. Canfield, A. S. Sefat, B. C. Sales, M. A. McGuire, and D. Mandrus, Phys. Rev. B **80**, 134523 (2009).
[45] Y. Xiao, Y. Su, R. Mittal, T. Chatterji, T. Hansen, C. M. N. Kumar, S. Matsuishi, H. Hosono, and Th. Brueckel, Phys. Rev. B **79**, 060504(R) (2009).
[46] Hironari Okada, Hiroyuki Takahashi, Yoshikazu Mizuguchi, Yoshihiko Takano, and Hiroki Takahashi, J. Phys. Soc. Jpn. **78**, 083709 (2009).
[47] Y. Xia, D. Qian, L. Wray, D. Hsieh, G. F. Chen, J. L. Luo, N. L. Wang, and M. Z. Hasan, Phys. Rev. Lett. **103**, 037002 (2009).
[48] E. Colombier, S. L. Bud'ko, N. Ni, and P. C. Canfield, Phys. Rev. B **79**, 224518 (2009).
[49] T. Goko, A. A. Aczel, E. Baggio-Saitovitch, S. L. Bud'ko, P. C. Canfield, J. P. Carlo, G. F. Chen, P. Dai, A. C. Hamman, W. Z. Hu, H. Kageyama, G. M. Luke, J. L. Luo, B. Nachumi, N. Ni, D. Reznik, D. R. Sanchez-Candela, A. T. Savici, K. J. Sikes, N. L. Wang, C. R. Wiebe, T. J. Williams, T. Yamamoto, W. Yu, and Y. J. Uemura, Phys. Rev. B **80**, 024508 (2009).
[50] J. T. Park, D. S. Inosov, Ch. Niedermayer, G. L. Sun, D. Haug, N. B. Christensen, R. Dinnebier, A. V. Boris, A. J. Drew, L. Schulz, T. Shapoval, U. Wolff, V. Neu, X. Yang, C. T. Lin, B. Keimer, and V. Hinkov, Phys. Rev. Lett. **102**, 117006 (2009).
[51] J. D. Jorgensen, B. Dabrowski, S. Pei, D. G. Hinks, L. Soderholm, B. Morosin, J. E. Schirber, E. L. Venturini, and D. S. Ginley, Phys. Rev. B **38**, 11337 (1988).
[52] S. H. Pan, J. P. O'Neil, R. L. Badzey, C. Chamon, H. Ding, J. R. Engelbrecht, Z. Wang, H. Eisaki, S. Uchida, A. K. Gupta, K.-W. Ng, E. W. Hudson, K. M. Lang, and J. C. Davis, Nature (London) **413**, 282 (2001).